Ahmadikia *et al.*
Journal of Materials Science: Materials Theory (2024) 8:4
https://doi.org/10.1186/s41313-024-00055-9

Journal of Materials Science: Materials Theory

RESEARCH Open Access

Designing Ti-6Al-4V microstructure for strain delocalization using neural networks

Behnam Ahmadikia[1*], Adolph L. Beyerlein[2], Jonathan M. Hestroffer[3], M. Arul Kumar[4] and Irene J. Beyerlein[1,3]

*Correspondence:
behnam_ahmadikia@ucsb.edu

[1] Department of Mechanical Engineering, University of California Santa Barbara, Santa Barbara 93106, CA, USA
[2] Department of Chemistry, Clemson University, Clemson 29634, SC, USA
[3] Materials Department, University of California Santa Barbara, Santa Barbara 93106, CA, USA
[4] Materials Science and Technology Division, Los Alamos National Laboratory, Los Alamos 87545, NM, USA

Abstract

The deformation behavior of Ti-6Al-4V titanium alloy is significantly influenced by slip localized within crystallographic slip bands. Experimental observations reveal that intense slip bands in Ti-6Al-4V form at strains well below the macroscopic yield strain and may serially propagate across grain boundaries, resulting in long-range localization that percolates through the microstructure. These connected, localized slip bands serve as potential sites for crack initiation. Although slip localization in Ti-6Al-4V is known to be influenced by various factors, an investigation of optimal microstructures that limit localization remains lacking. In this work, we develop a novel strategy that integrates an explicit slip band crystal plasticity technique, graph networks, and neural network models to identify Ti-6Al-4V microstructures that reduce the propensity for strain localization. Simulations are conducted on a dataset of 3D polycrystals, each represented as a graph to account for grain neighborhood and connectivity. The results are then used to train neural network surrogate models that accurately predict localization-based properties of a polycrystal, given its microstructure. These properties include the ratio of slip accumulated in the band to that in the matrix, fraction of total applied strain accommodated by slip bands, and spatial connectivity of slip bands throughout the microstructure. The initial dataset is enriched by synthetic data generated by the surrogate models, and a grid search optimization is subsequently performed to find optimal microstructures. Describing a 3D polycrystal with only a few features and a combination of graph and neural network models offer robustness compared to the alternative approaches without compromising accuracy. We show that while each material property is optimized through a unique microstructure solution, elongated grain shape emerges as a recurring feature among all optimal microstructures. This finding suggests that designing microstructures with elongated grains could potentially mitigate strain localization without compromising strength.

Keywords: Titanium alloys, Strain localization, Targeted properties, Data-driven optimization, Slip bands

Introduction

As the most common wrought titanium alloy, Ti-6Al-4V finds extensive applications in industries such as aerospace, energy, biomedical, and chemical processing (Boyer 2010; Williams and Boyer 2020). Like many other titanium alloys, plastic deformation in Ti-6Al-4V is mainly realized via formation of localized slip bands (Zhang et al.

2010; Echlin et al. 2016; Hémery et al. 2018; Lunt et al. 2016). Unlike pure titanium, however, the alloy does not readily twin unless subjected to very high strain levels during severe plastic deformation processes (Wang and Liu 2016; Yapici et al. 2006). At low and moderate strain levels, different slip systems including prismatic, basal, and pyramidal are commonly observed in Ti-6Al-4V (Echlin et al. 2016; Hémery et al. 2018).

Although the formation of slip bands is the main underlying mechanism limiting material ductility and formability, the same phenomenon is believed to be responsible for crack initiation and propagation and, ultimately, material failure (Ghoniem et al. 2003). Ti-6Al-4V titanium alloy is not excluded from this trade-off between strength and toughness. While several theories have been proposed to explain it, a recent experiment on a wide range of polycrystalline materials with several crystal structures revealed that the trade-off has its root in microscopic strain localization within slip bands (Stinville et al. 2022). It was shown that the reason why toughness of a material does not scale with its macroscopic strength is that stronger materials, i.e., with a higher yield strength, show a higher tendency to localize strain within intense slip bands. Several studies have shown that stress (or strain) concentrations associated with these localized slip bands can promote either slip transmission across the grain boundary or the development of microvolumes at the slip band/grain boundary junction (Ahmadikia et al. 2021, 2023; Papanikolaou et al. 2017). These types of localized events can contribute to crack initiation, which is the first step in compromising material toughness (Erel et al. 2017).

Over the past few decades, an extensive number of experimental studies have characterized slip bands in Ti-6Al-4V titanium alloy (Echlin et al. 2016; Hémery et al. 2018; Lunt et al. 2016; Lavogiez et al. 2018; Ren et al. 2017). Most relevant to our work, *in situ* high-resolution scanning electron microscope, digital image correlation (HR SEM-DIC) was employed to investigate the relationship between strain localization and the microstructure of a rolled Ti-6Al-4V plate (Echlin et al. 2016). It was found that not only did slip bands form before the macroscopic yield point, but they serially transmitted from one grain to another within micro-textured zones, creating a long-range plastic strain localization phenomenon. Such a chain of intense localized slip bands has been correlated with a high frequency of crack initiation events in low cycle fatigue of the alloy (Bridier et al. 2008; Le Biavant et al. 2002). A separate *in situ* SEM investigation of slip transfer in Ti-6Al-4V also confirmed that slip transfer occurs well below the conventional 0.2% yield stress (Hémery et al. 2018). It was further revealed that the likelihood of slip transmission in the alloy significantly increases when there is a good alignment between the incoming and outgoing slip systems, and a high resolved shear stress on the outgoing slip system. The first condition emphasizes the role of grain orientation or texture, while the second manifests the critical role of the grain neighborhood on slip localization and transmission in Ti-6Al-4V. In conclusion, experimental studies confirm that the development and connectivity of slip bands in titanium alloys, including Ti-6Al-4V, adversely affect their mechanical properties (Echlin et al. 2016; Dawson et al. 2021; Hémery et al. 2019). Motivated by these studies, a key question is what combination of microstructural features promote slip localization in Ti-6Al-4V and, perhaps more importantly, what ideal set of features would give rise to a delocalized accommodation of the applied strain in this alloy?

Aside from experimental works, a few computational studies investigated the development of slip bands in Ti-6Al-4V, presenting an acceptable agreement between simulation and experimental results (Zhang et al. 2010; Ahmadikia et al. 2021). However, they were limited to a single microstructure and did not explore the effect of microstructure on slip localization in the alloy. Given that there are many parameters involved, such as material parameters, microstructural features, loading conditions, etc., the space of contributing factors to material properties is outstandingly high dimensional that pure computational exploration would not be practical. In light of this, data-driven and machine learning approaches have recently been used to predict polycrystalline materials properties based on their microstructure characteristics (Liu et al. 2015; Mangal and Holm 2019; Herriott and Spear 2020; Dai et al. 2021; Shu et al. 2022; Pagan et al. 2022; Hestroffer et al. 2023). Most relevant to our work, a heterogeneous grain graph attention model (HGGAT) capable of realizing high-order feature embedding of the microstructure was employed to mine the relationship between the structure and elongation in magnesium alloys (Shu et al. 2022). Using a graph neural network (GNN) model trained on simulation results from crystal elasticity finite element method (CEFEM), grain-scale elastic response of polycrystalline Ti-7Al titanium alloy was predicted (Pagan et al. 2022). Retaining fundamental features of grains including their crystallographic orientation, size, and neighborhood, a similar GNN model was used in a separate study to predict overall stiffness and strength of $\alpha-$Ti microstructures with varying textures (Hestroffer et al. 2023). Finally, random forest based machine learning models were used to predict stress hot-spot formation in 2D hexagonal close-packed (HCP) microstructures (Mangal and Holm 2019). It was found that both the crystallography, i.e., texture, and geometry based features are required to predict stress hot-spots.

While these machine learning models have demonstrated promising accuracy levels in predicting mechanical properties, they mainly focus on the overall material properties, such as average stress, and overlook the local plastic deformation events that play a critical role in the response of the material and its failure. In the case of slip bands, it is only recently that computational tools that can model these localized events in 3D microstructure settings have been developed and validated. Furthermore, most relevant machine learning studies to date are limited to predicting material properties from its microstructure, leaving the microstructure optimization for superior properties unaddressed.

In this paper, we aim to identify the microstructural features that would minimize strain localization in Ti-6Al-4V titanium alloy. To this end, we strategically combine micromechanical simulations, graph networks, and neural network models to develop a framework significantly more efficient than conventional computational tools and more interpretable than machine learning methods, such as GNNs, that are commonly used to predict the properties of polycrystalline aggregates. First, slip band fast Fourier transform (SB-FFT) simulations are conducted on a dataset of 3D microstructures, and the resulting data is used to train surrogate neural network models. Grain neighborhood and connectivity within the polycrystals are accounted for via graph-based representation of polycrystalline microstructures. The surrogate neural network models exhibit satisfactory predictive performance for localization-based properties, such as the ratio of slip accumulated in the band to that in the matrix, fraction of total applied

strain accommodated by slip bands, and spatial connectivity of slip bands throughout the microstructure. These models are then used to generate synthetic data, providing an enhanced dataset ideal for a grid search optimization. Using only a few key features, such as texture and average grain size, to describe a 3D microstructure enhances robustness and reduces computational cost compared to alternative approaches like CNN and GNN. Our optimization results find that each material property is optimized through a unique microstructure solution. All optimal solutions, however, share elongated grain shape as one of their features, rendering elongated grains as a valuable target parameter for the design of Ti-6Al-4V microstructures with reduced strain localization that can potentially mitigate the strength/toughness trade-off.

Methods

Figure 1 shows the workflow for the data-driven microstructure design approach used in this work. We combine explicit slip band micromechanical simulations on 3D polycrystals with neural network (NN) models to design an optimal Ti-6Al-4V microstructure featuring strain delocalization. We first generate a dataset of 3D polycrystals with different microstructural characteristics and perform crystal plasticity simulations to calculate the mechanical response of each polycrystal, from a localization perspective. We then formulate a set of localization-based properties to optimize, with respect to our goal of delocalizing strain. Subsequently, we design and tune separate NN models to predict these properties for a microstructure, given its characteristics such as texture, grain size and shape. With the high accuracy of these models established, we employ them to generate additional data to enhance our initial dataset of 3D microstructures. Finally, utilizing the expanded dataset, we perform a grid search optimization to identify optimal microstructures, each contributing to the improvement of a specific localization-based property.

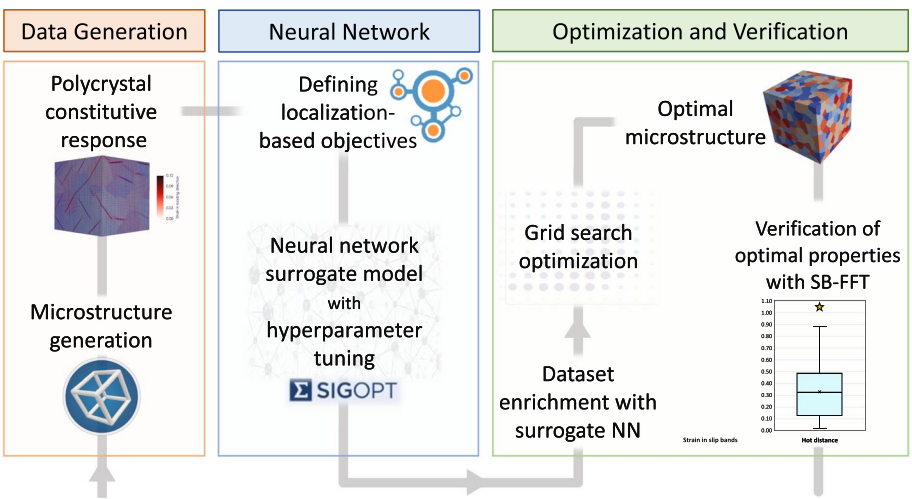

Fig. 1 Flowchart for design of a microstructure with limited slip localization and transmission likelihood. The workflow consists of data generation using DREAM3D and explicit slip band micromechanical calculations, design of surrogate neural network for predicting localization-based properties, and microstructure optimization via simple grid search

Data generation and model set-up

Our dataset comprises a total of 360 polycrystalline microstructures, each generated in DREAM3D (Groeber et al. 2014) with a set of unique microstructural features. The first two features included are the mean (μ) and standard deviation (σ) of the grain size distribution calculated from all grains within the microstructure. To accommodate a wide range of grain sizes, we consider $\mu = [2, 2.33, 2.66, 3, 3.5]$. Furthermore, any value from [0.001, 0.01, 0.1, 0.3] can be assigned to σ, introducing very small to significant variations in grain size within the microstructure. It should be noted that the parameter μ does not represent the actual grain size mean but the average value of the log-normal grain size distribution. Similarly, σ is the standard deviation of the log-normal distribution, i.e.,

$$\mathrm{ESD}_{\mathrm{ave}} = \exp(\mu + \sigma^2/2) \tag{1}$$

where ESD_{ave} can be deemed as the actual grain size in terms of equivalent sphere diameter. The set of possible values for μ, therefore, yields grains that may have an *ESD* of approximately 7.4, 10.3, 14.3, 20.1, and 33.1 voxels. Figure 2 shows how μ and σ control the overall size and dispersion in size of the grains within the microstructure.

Next, we include in our features the morphology of the grains by allowing either equiaxed or rolled grains to comprise the microstructure. This feature is controlled by the aspect ratio (AR) of the grains, to which any value from [1, 3, 8] can be assigned. Figure 3 shows example microstructures with equiaxed (AR = 1) and elongated grains (AR = 3, 8). Although larger values of AR can be considered, they may introduce problems during the compilation and packing of grains in DREAM3D.

The fourth and last microstructural feature included is the texture. Figure 4 presents the pole figures for six unique textures from which the orientation of the grains is sampled. Among them, texture C is an experimentally rolled titanium texture (Wang et al. 2020) and texture F is a uniformly random (no) texture. The remaining textures are synthetic and inspired by the literature on titanium alloys (Priddy et al. 2017; Peters et al. 1983; Peters et al. 1984; Lütjering et al. 1998; Smith 2013).

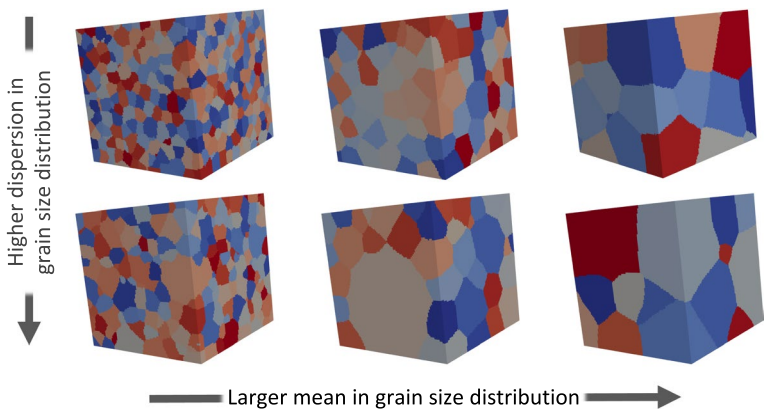

Fig. 2 Variations in the mean and standard deviation of the grain size distribution within a few example microstructures. Columns from left to right correspond to $\mu = 2$, 2.66, and 3.5, while the top and bottom rows show polycrystals with $\sigma = 0.001$and 0.1, respectively

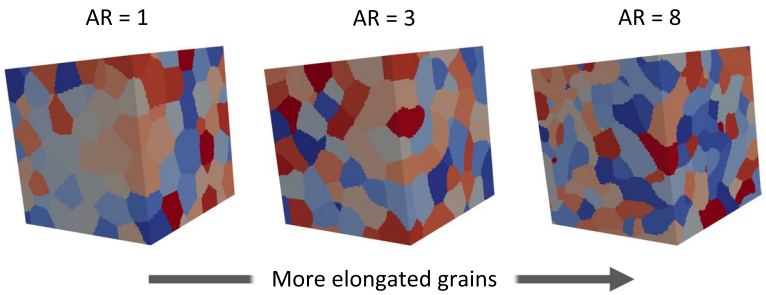

Fig. 3 Variation in grain shape is manifested by a few example microstructures. From left to right, polycrystals are generated with a grain aspect ratio of AR = 1(equiaxed), 3 (elongated), and 8 (severely elongated). In polycrystals with AR > 1, the long axis of grains are randomly oriented

Explicit slip band modeling

Each 3D polycrystal generated by DREAM3D is discretized into $100 \times 100 \times 100$ ($x \times y \times z$) voxels, as shown in Fig. 5a. A narrow volume serving as the slip band domain is manually added to each grain within the microstructure. In actuality, where slip bands form is random and determined by a number of defect and local stress variables. In the model, the designated slip plane in each grain is located at the grain centroid to reduce randomness, to simplify the microstructure-generation process, and to ensure that slip can fully localize, provided that the loading and neighborhood conditions favor such localization. Moreover, each slip plane is spatially oriented such that it aligns with the grain's most favorable slip system, given the macroscopic loading direction. Material parameters for Ti-6Al-4V including the elastic constants and critical resolved shear stress (CRSS) for different slip modes are listed in Table 1. Considering that prismatic slip has the lowest CRSS value, the slip plane in each grain lies on the prismatic plane with the highest Schmid factor, as shown in Fig. 5b. The microstructure is surrounded by a 20-voxel-thick homogeneous layer with uniformly distributed crystal orientations in all directions to ensure that the spatially resolved micromechanical fields are unaffected by the periodic nature of the imposed boundary conditions (Fig. 5c).

To allow the slip bands to develop in each polycrystal, we employ the SB-FFT model (Ahmadikia et al. 2021). SB-FFT is a full-field, crystal plasticity model that extends the elasto-viscoplastic fast Fourier transform (EVP-FFT) technique (Lebensohn et al. 2012), to permit the development of discrete, crystallographic slip bands in grains. These models have been extensively used in simulations of slip bands (Ahmadikia et al. 2021, 2023, 2024; Wang et al. 2016; Marano et al. 2019; Marano and Gélébart 2020) and deformation twinning (Kumar et al. 2016a, b, 2019; Kumar and Beyerlein 2020; Hu et al. 2021). We review them briefly here and refer the reader to the original articles, Lebensohn et al. (2012) and Ahmadikia et al. (2021), for more detailed information about these computational schemes.

The constitutive relationship of an elasto-viscoplastic material is given by,

$$\boldsymbol{\sigma}(\mathbf{x}) = \mathbf{C}(\mathbf{x}) : \boldsymbol{\varepsilon}^{\mathrm{e}}(\mathbf{x}) = \mathbf{C}(\mathbf{x}) : \left(\boldsymbol{\varepsilon}(\mathbf{x}) - \boldsymbol{\varepsilon}^{\mathrm{p}}(\mathbf{x})\right) \tag{2}$$

where $\boldsymbol{\sigma}(\mathbf{x})$ is the Cauchy stress tensor, $\mathbf{C}(\mathbf{x})$ contains anisotropic elastic constants, and $\boldsymbol{\varepsilon}(\mathbf{x})$, $\boldsymbol{\varepsilon}^{\mathrm{e}}(\mathbf{x})$, and $\boldsymbol{\varepsilon}^{\mathrm{p}}(\mathbf{x})$ represent the total, elastic, and plastic strain tensors, respectively,

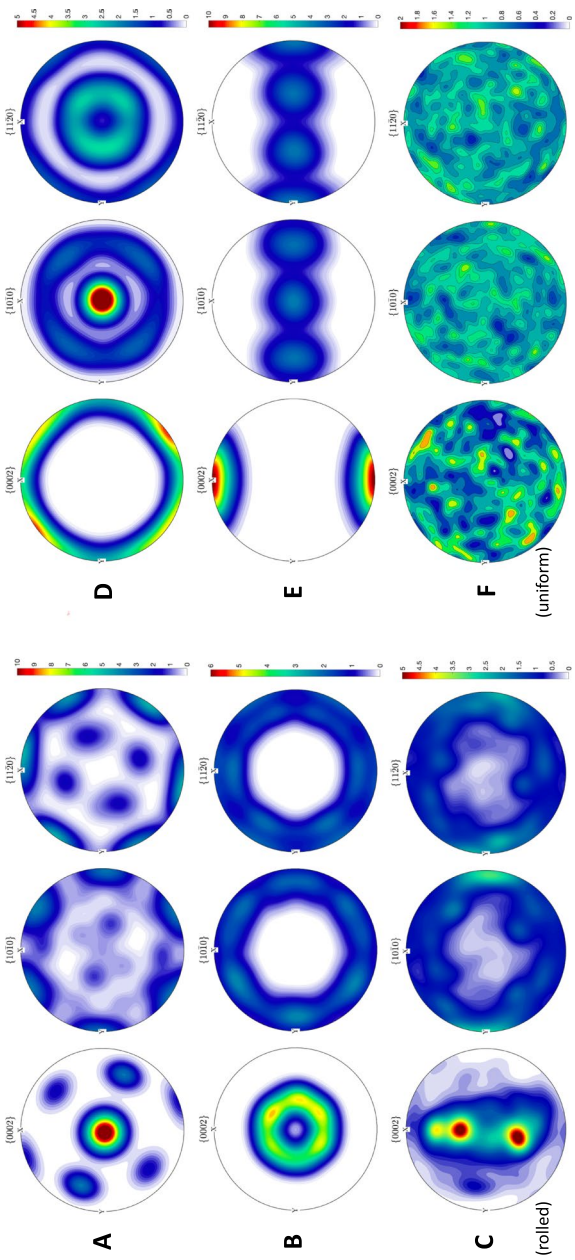

Fig. 4 Pole figures for textures A through F used for the assignment of orientation to the grains within each microstructure. Textures C and F are experimentally rolled and uniformly random (no) textures, respectively. Intensities are plotted as multiples of random distribution (MRD)

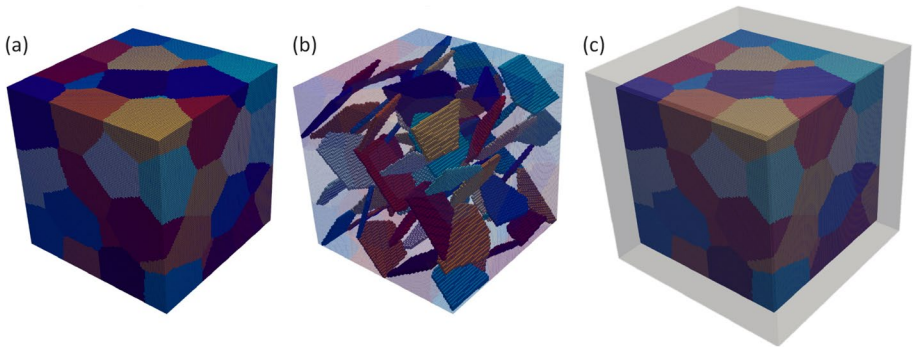

Fig. 5 **a** An example 3D polycrystal is generated by DREAM3D and discretized into 100 × 100 × 100 ($x \times y \times z$) voxels. **b** A narrow slip band domain is added to each grain, aligned with the most favorable prismatic slip system in the grain. **c** The polycrystal is surrounded by a 20-voxel-thick buffer layer in all directions. This layer is homogeneous and comprised of uniformly distributed crystal orientations

calculated at any material point $\mathbf{x}$. An implicit time discretization scheme, evaluates the stress state in material point $\mathbf{x}$ at time $t + \Delta t$ as follows:

$$\boldsymbol{\sigma}^{\mathrm{t}+\Delta\mathrm{t}}(\mathbf{x}) = \mathbf{C}(\mathbf{x}) : \left(\boldsymbol{\varepsilon}^{\mathrm{t}+\Delta\mathrm{t}}(\mathbf{x}) - \boldsymbol{\varepsilon}^{\mathrm{p},\,\mathrm{t}}(\mathbf{x}) - \dot{\boldsymbol{\varepsilon}}^{\mathrm{p},\,\mathrm{t}+\Delta\mathrm{t}}\left(\mathbf{x}, \boldsymbol{\sigma}^{\mathrm{t}+\Delta\mathrm{t}}\right)\Delta\mathrm{t}\right) \tag{3}$$

Following the Hutchinson-type simple power law constitutive equation, the viscoplastic strain-rate tensor $\dot{\boldsymbol{\varepsilon}}^{\mathrm{p}}(\mathbf{x})$ is calculated given the stress tensor $\boldsymbol{\sigma}(\mathbf{x})$ through a sum over N active slip systems, as:

$$\dot{\boldsymbol{\varepsilon}}^{\mathrm{p}}(\mathbf{x}) = \sum_{\mathrm{s}=1}^{\mathrm{N}} \mathbf{m}^{\mathrm{s}}(\mathbf{x})\dot{\gamma}^{\mathrm{s}}(\mathbf{x}) = \dot{\gamma}_0 \sum_{\mathrm{s}=1}^{\mathrm{N}} \mathbf{m}^{\mathrm{s}}(\mathbf{x}) \left(\frac{|\mathbf{m}^{\mathrm{s}}(\mathbf{x}) : \boldsymbol{\sigma}(\mathbf{x})|}{\tau_{\mathrm{c}}^{\mathrm{s}}(\mathbf{x})}\right)^{\mathrm{n}} \mathrm{sgn}\left(\mathbf{m}^{\mathrm{s}}(\mathbf{x}) : \boldsymbol{\sigma}(\mathbf{x})\right) \tag{4}$$

where $\dot{\gamma}^{\mathrm{s}}(\mathbf{x})$ and $\tau_{\mathrm{c}}^{\mathrm{s}}(\mathbf{x})$ are respectively the shear rate and the critical resolved shear stress (CRSS) for slip system s at material point $\mathbf{x}$, $\dot{\gamma}_0$ is a normalization factor, and n is the stress exponent. Finally, $\mathbf{m}^{\mathrm{s}} = (\mathbf{b}^{\mathrm{s}} \otimes \mathbf{n}^{\mathrm{s}} + \mathbf{n}^{\mathrm{s}} \otimes \mathbf{b}^{\mathrm{s}})/2$ denotes the Schmid tensor calculated for slip system s, where unit vectors $\mathbf{b}^{\mathrm{s}}$ and $\mathbf{n}^{\mathrm{s}}$ show the direction of the Burgers vector and slip plane normal, respectively.

The SB-FFT model used in this work allows for incremental development of a discrete slip localization within a grain. This is accomplished by assigning a softening, rate-dependent constitutive law to the material points within a preselected narrow domain, i.e., the slip band domain as shown in Fig. 5b. Prior selection of such domain, however, does not necessarily enforce the slip band to develop. Instead under an applied macroscopic strain, the strain within the domain is available to evolve, at a rate that depends not only on its softening law, but also the properties of the host grain and its local neighborhood. Slip resistance in material points outside of the slip band domain, referred to as the *matrix*, remains constant throughout the simulation. The rate by which the critical resolved shear stress τ_c^{s} for any slip system s in the slip band domain decays depends linearly on the rate of slip ($\dot{\gamma}^{\mathrm{s}}$) accumulated on that system, as in the following:

$$\tau_c^{\mathrm{s},\,\mathrm{t}+\Delta\mathrm{t}}(\mathbf{x}) = \begin{cases} \tau_c^{\mathrm{s},\,\mathrm{t}}(\mathbf{x}) - D_0\tau_c^{\mathrm{s},\,\mathrm{t}}(\mathbf{x})\left|\dot{\gamma}^{\mathrm{s},\,\mathrm{t}}(\mathbf{x})\right|\Delta t & : \ \mathbf{x} \in \text{SB domain} \\ \tau_c^{\mathrm{s},\,\mathrm{t}}(\mathbf{x}) = \tau_c^{\mathrm{s},\,0}(\mathbf{x}) & : \ \mathbf{x} \notin \text{SB domain} \end{cases} \tag{5}$$

Table 1 Elastic constants (Simmons and Wang 1971), c/a ratio (Yoo 1981), softening coefficient D_0, and CRSS values for different deformation modes (Bridier et al. 2009) for Ti-6Al-4V

Material	Elastic constants (GPa)					c/a ratio	D_0	CRSS values for deformation modes (MPa)		
	C_{11}	C_{22}	C_{13}	C_{33}	C_{44}			basal $< a >$	prismatic $< a >$	pyramidal I $< c + a >$
Ti-6Al-4V	162.4	92.0	69.0	180.7	46.7	1.588	64	420	370	590

In (5), coefficient D_0 is a material constant that controls the rate of softening. D_0 is set to 64, consistent with the model calibration performed for Ti-6Al-4V alloy elsewhere (Ahmadikia et al. 2021). The polycrystal setup is strained along the y-axis, up to a macroscopic strain of 1%, while the normal stress components along the x- and z-axis are enforced to be zero. To avoid numerical instabilities, a lower limit for τ_c^s equal to 10% of its initial value is set for all slip systems.

Defining localization-based property objectives

We begin this section by presenting results of the micromechanical simulations with SBFFT model from which we define three objectives related to the localization behavior of the material to achieve in our optimization process. Figure 6a shows the distribution of the normal strain along the loading direction resolved on two surfaces of an example microstructure subjected to 1% total strain. While strain localization within slip band domains is evident throughout the sample, localization intensity varies from one grain to another and, more interestingly, some grains did not develop significant localization. Under the 1.0% far-field strain applied to the polycrystal, the simulated range for strain within the slip band domains is consistent with the experimental observations from the same alloy (Echlin et al. 2016). Furthermore, the strain map in Fig. 6a demonstrates spike in strain within some grains where the slip band active in a neighboring grain impinged on the shared grain boundary. The study Ahmadikia et al. (2021) report similar localized stress concentrations ahead of an active slip band. Such stress or strain concentrations can potentially trigger a new slip/twin band in the grain (Ahmadikia et al. 2023). It can explain the formation of a long chain of bands seen to eventually lead to material failure (Echlin et al. 2016).

To better understand and compare different localization responses, Fig. 6b and c shows the histogram of the strain in loading direction across all grains from two microstructures, one sampled from texture D and the other from texture E. In these plots, orange and blue bars represent the strain accommodated by the matrix and slip band domain, respectively. Figure 6b indicates that most grains within the polycrystal accommodate a strain level approximately equal to the 1.0% far-field strain. Furthermore, in a large fraction of grains, both the matrix and the slip band domain experience the same strain levels, manifesting this case as a microstructure with low localization or *delocalized* strain state. In stark contrast, Fig. 6c presents a microstructure in which most grains accommodate less than 1.0% strain in their matrix and significantly larger strains in their slip band domains. We consider this case a polycrystal with a high degree of localization.

The key question to address next concerns the combination of microstructural features that lead to a localized strain response. More importantly, is there an ideal set of features that gives rise to the accommodation of the applied strain in a delocalized manner? To address these questions, we define and formulate a set of property objectives associated with the localization response of the polycrystal. Intuitively, the first quantity to consider is the *slip ratio (SR)*, which evaluates the ratio of the strain accommodated by the slip band domain to that accommodated by the parent matrix in each grain. A case of perfectly homogeneous deformation yields $\mathrm{SR} = 1$, while $\mathrm{SR} > 1$ indicates some extents of localization. Figure 7a shows the cloud distribution of the strain in loading direction in two grains within the same microstructure. The

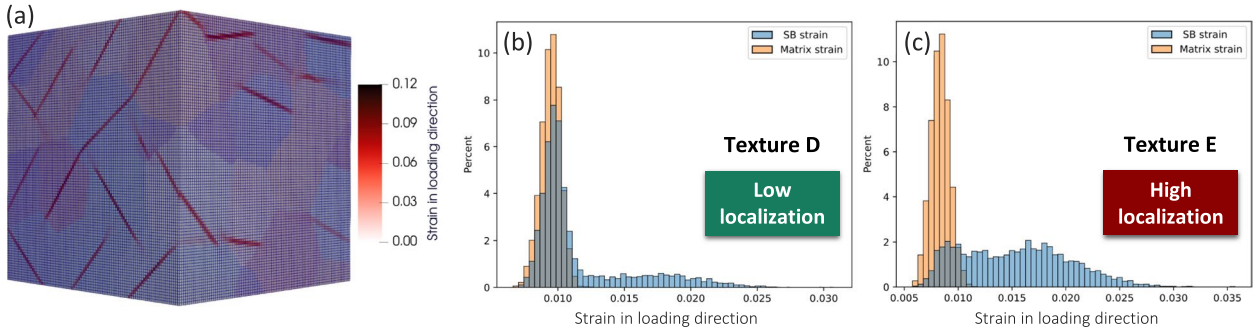

Fig. 6 **a** Distribution of the normal strain along the loading direction for an example microstructure subjected to 1% total strain. Localization intensity varies from one grain to another throughout the microstructure. **b** Histogram of the strain in loading direction across all grains within a microstructure sampled from texture D shows a delocalized strain state. (c) A same histogram for a microstructure sampled from texture E indicates a high degree of localization of slip within slip band domains

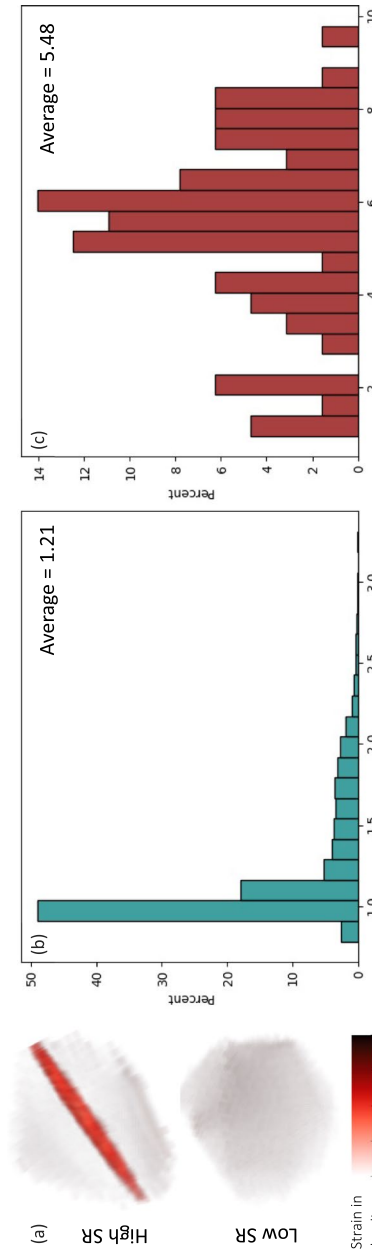

Fig. 7 **a** Distribution of the strain in loading direction contrasts the slip ratios in two grains within the same microstructure. **b** Histogram of the slip ratio (SR) across all grains within a microstructure ($\mu = 2$, AR = 8, Tex = D) shows a delocalized strain state. **c** A same histogram for a different microstructure ($\mu = 3.5$, AR = 1, Tex = E) indicates a high degree of localization evidenced by a majority of the bars at SR > 1

top grain manifests a strong, pronounced slip localization within its band domain, hence a high SR, while the bottom grain accommodates the imposed strain homogeneously with SR $\simeq 1$. Similar to the comparison made in Fig. 6, the histograms in Fig. 7b and c distinguish a microstructure with a delocalized strain state ($SR_{ave} = 1.21$) from a highly localized strain response ($SR_{ave} = 5.8$). Motivated by these results, we therefore define our first objective to design a microstructure with minimal slip ratio when averaged over all grains, i.e.,

$$\text{minimize}_{\mathbf{f}\in\{\mu,\sigma,AR,Tex\}}\ SR_{ave} = \frac{1}{N}\sum_{N}\frac{\varepsilon_{SB}}{\varepsilon_{M}}, \tag{6}$$

where $\mathbf{f}$ is the feature vector including grain size average (μ), its standard deviation (σ) and shape (AR), and the texture (Tex) of the microstructure encompassing N grains. Furthermore, ε_{SB} and ε_{M} are respectively the strain in loading direction within the slip band domain and the matrix of each grain. For simplicity, we hereinafter drop the subscript "ave" and refer to the average slip ratio for a microstructure as "SR".

Next, we define as our second localization-based property the fraction of total applied strain that is accommodated within all slip band domains throughout the microstructure, and denote it by E_{inSB}. While this property was anticipated to be closely correlated with the SR defined earlier, our statistical analysis revealed that it is not entirely the case as the correlation between SR and E_{inSB} is not monotonically increasing. For instance, within the dataset there is a microstructure with SR < 2 and $E_{inSB} \simeq 0.5$, while another microstructure accommodates a significantly lower fraction of the applied strain within its slip bands ($E_{inSB} \simeq 0.2$) with an SR value of 4. The key distinction between these two cases is that the former tends to accumulate the larger share of the applied strain within its many activated slip bands such that each band is only moderately localizing. On the contrary and perhaps due to the lack of enough active slip bands, the latter microstructure accommodates the imposed deformation via its few, yet highly intense slip bands. Considering that a lower E_{inSB} would mean that a larger share of the applied strain is accommodated homogeneously within the matrix, we can define the second objective to design a microstructure that minimizes the fraction of strain in slip bands, i.e.,

$$\text{minimize}_{\mathbf{f}\in\{\mu,\sigma,AR,Tex\}}\ E_{inSB} = \frac{\sum_{N}\varepsilon_{SB}}{\sum_{N}(\varepsilon_{M}+\varepsilon_{SB})}. \tag{7}$$

Finally, we consider as our third localization-based property the spatial connectivity of the slip bands activated throughout the microstructure. As mentioned in the Introduction, serial transmission and connection of slip bands across the polycrystal has been experimentally evidenced to be the primary cause for initiation, easy coalescence, and growth of micro-cracks in Ti-6Al-4V titanium alloy (Echlin et al. 2016; Le Biavant et al. 2002). Therefore, an intuitive approach to delay crack formation and ultimate failure of the material is to have slip bands activated far from one another within the microstructure. This will minimize the risk of intense slip bands coalescing to form detrimental long-range plastic strain localization. A simple approach for defining a relevant property is to consider the Euclidean distance between any two

slip bands in the microstructure. Nevertheless, doing so would fail to take account of grain connectivity within the microstructure. It has been demonstrated in previous research that the stress concentration ahead of an active slip band can trigger a new set of bands in the grain neighbor in a transmission event across the shared grain boundary (Ahmadikia et al. 2021, 2023). Experimental observations from Ti-6Al-4V also emphasize the role of grain connectivity in the formation of long-range strain localization (Echlin et al. 2016). For a slip band to link with another, it needs to serially transmit from one grain to the nearest neighbor, naturally following the grain connectivity within the microstructure. Therefore, using Euclidean distance between two grains is clearly not ideal. To circumvent this and to account for natural progression of slip bands through the microstructure, we apply a graph network to each polycrystal, using the Python package NetworkX (Hagberg et al. 2008). Figure 8a shows a simplified version of such a graph, including only surface-visible grains in the polycrystal. Each grain is represented by a node located at the centroid of the grain. There is an edge between two nodes if the two corresponding grains are nearest neighbors. It follows that a more reasonable approach to account for the spatial distance between two grains within the microstructure is to evaluate the shortest path between their corresponding nodes in the graph.

We further incorporate slip band intensity into our third localization-based property to place a greater emphasis on intense localization events within the microstructure. In Fig. 8a grains within which a more intense slip band is activated are visualized by larger nodes with darker shades of red. Each node also retains the slip ratio (SR) of the grain as its attribute. When calculating the distance between the two most intense slip bands, SR_1 and SR_2 in this example, the shortest path indicated by bold arrows is divided by the product of slip ratio of the two grains. This approach yields a lower adjusted distance between two intense slip bands, and therefore rating them more alarming, compared to two slip bands with the same physical distance but lower intensities. Finally, the adjusted distance is normalized by the average grain size, ESD_{ave}, to obtain a quantity

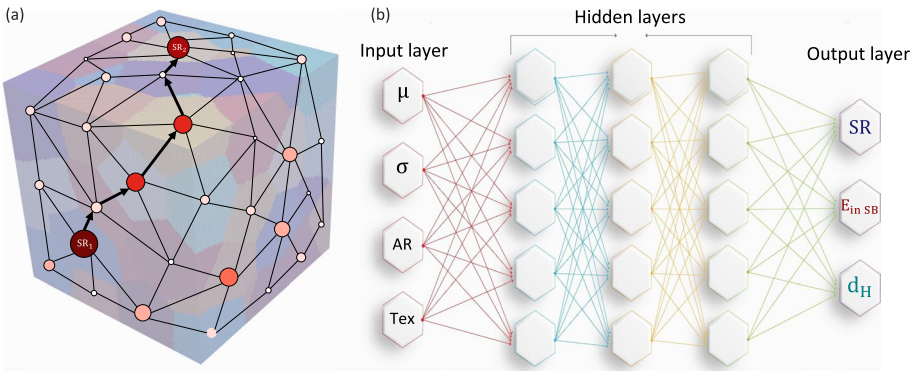

Fig. 8 **a** A simplified version of a graph including only surface-visible grains in the polycrystal. Each node represents a grain, with its size and color intensity proportional to the grain's slip ratio. An edge between two nodes indicates that two grains are nearest neighbors. Considering the grain neighborhood, bold arrows show the shortest path between two grains with intense slip bands. **b** Overall architecture of the neural network model developed here, which includes an input layer, multiple fully-connected hidden layers with ReLU activation function, and an output regression layer. The output layer has only one neuron to predict any of the three properties

that is comparable across fine and coarse grain polycrystals. In a sense, the normalized quantity indicates the number of grains across which one slip band needs to traverse to connect to the other band. We thus define the third objective to design a microstructure that maximizes the *hot distance* (d_H), the average normalized, adjusted distance between slip bands, as in the following,

$$\text{maximize}_{\mathbf{f}\in\{\mu,\sigma,AR,Tex\}}\ d_H = \frac{1}{ESD_{ave}N}\sum_{i,j\in[N]}\frac{shortest\ path\ between\ grains\ i,j}{SR_iSR_j}. \tag{8}$$

Neural network model and microstructure optimization

With the four microstructural features considered as input parameters and three localization-based properties introduced in (6), (7), and (8) as labels, this section describes the design and optimization of three separate neural network (NN) models to predict the localization response of a polycrystal based on its microstructure.

NN architecture and hyper-parameter tuning

Figure 8b shows the overall architecture of the NN we employ to predict localization in the polycrystalline deformation response. The NN developed here is a simple multilayer perceptron (MLP) consisting of an input layer with four neurons, multiple fully-connected hidden layers with rectified linear unit (ReLU) activation function, and a post-processing regression layer. Alternatively, more smooth activation functions can be used that provide the possibility for application of non-gradient optimization methods. However, due to its simplicity, ReLU activation function is used in the present work. Parameters of the model associated with fully-connected layers are trained with the Adam adaptive learning rate optimization algorithm (Kingma and Ba 2014), using mean-squared error (MSE) as the loss function. We assign 70% of the data for training, with the remaining 30% kept unseen by the model for testing to assess its generalization capability. From the training data, 10% is reserved for cross-validation.

To optimize the performance of our neural network model, we conduct hyper-parameter tuning, focusing on all parameters except the base architecture of the model. These parameters include number of layers, learning rate, number of epochs, batch size, and number of neurons in each layer. We employ SigOpt (Clark and Hayes 2019) and choose the MSE as our loss metric. SigOpt is an optimization tool that explores a grid of potential values for each hyper-parameter, in order to minimize the loss via Bayesian optimization. Table 2 provides a summary of the parameters and their respective potential values. For each NN, we perform a total of 300 separate experiments, each employing a unique hyper-parameter combination. Upon the completion of all experiments, we select the top candidate model to continue our analysis with the prediction of the localization response of a polycrystal. Listed in Table 2 are also the optimal values of hyper-parameters that produce a NN model with the lowest error for predicting each property.

Surrogate NN and grid search optimization

With the basics of the NN model established and its hyper-parameters optimized to produce the lowest error, we train each model on a subset of our dataset of 3D polycrystalline microstructures. To reiterate, each model receives four features as input, including

Table 2 Hyper-parameters of the neural network optimized for predicting each localization-based property. Listed are sets of possible values for each as well as the optimal values determined via Bayesian optimization using SigOpt

		Optimal values		
Hyper-parameter	**Possible values**	**SR**	$\mathbf{E_{inSB}}$	$\mathbf{d_H}$
Number of layers	[2, 3, 4, 5, 6]	5	2	6
Learning rate	$[1, 5, 10, 50, 100] * 10^{-4}$	$5 * 10^{-3}$	$5 * 10^{-3}$	10^{-3}
Number of epochs	[64, 128, 256, 512, 1024, 2048]	2048	2048	256
Batch size	[8, 16, 32, 64]	64	16	32
Size of layer 1	[8, 16, 32, 64]	8	16	64
Size of layer 2	[16, 32, 64, 128, 256]	128	256	256
Size of layer 3	[16, 32, 64, 128, 256]	128	-	128
Size of layer 4	[16, 32, 64, 128, 256]	128	-	256
Size of layer 5	[16, 32, 64, 128]	16	-	32
Size of layer 6	[8, 16, 32, 64]	-	-	16

the average and standard deviation of the grain size distribution, grain shape, and texture. The output for each model is one property among the slip ratio (SR), strain in slip bands (E_{inSB}), or hot distance (d_H). Once each NN is trained, we apply it to the test portion of the dataset kept unseen by the model, to evaluate its accuracy in predicting the localization-based property based on the characteristics of the microstructure. As listed in Table 2, each NN model is optimized in performance with a unique hyper-parameter configuration. We use the same approach for training, evaluation, and testing all models.

Figure 9 shows how NN model predictions compare with the true values calculated via SB-FFT micromechanical simulations for the test data. Overall, all three models exhibit acceptable performance, with an R^2 score of at least 0.95 and MSE of 0.033, at highest. Not only does such a high accuracy rate qualify these models as reliable tools for predicting localization-based material properties given the characteristics of a microstructure, but it provides the opportunity to rapidly enrich our dataset by generating additional pairs of features and labels, typically required for most optimization techniques. This advantage is more acknowledged when comparing the time it takes to run a micromechanical simulation on a 3D microstructure with a size of $100 \times 100 \times 100$ voxels (~36 hours on a machine with 2.6 GHz 6-Core Intel Core i7 processor, 16GB RAM, and MacOS v.10.15 operating system) with the time it takes for a NN model to do the same task in seconds.

Having separate models trained and successfully tested for each property, we then use these surrogate models to generate a large dataset of microstructural features and their corresponding material properties. The enriched dataset comprises approximately 1.5M sample microstructures, compared to our initial limited dataset of 360 microstructures generated with DREAM3D and SB-FFT simulations. The available range for each microstructural feature is extended in the enriched dataset, except for the texture for which we still use the six textures presented in Fig. 4. Particularly, the average grain size (ESD_{ave}) can take any value between 5 and 100 voxels, with an increment of 0.5. The range for grain aspect ratio (AR) extends to any integers between 1 and 30, and standard deviation of the grain size log-normal distribution can vary in increments of 0.02. We therefore

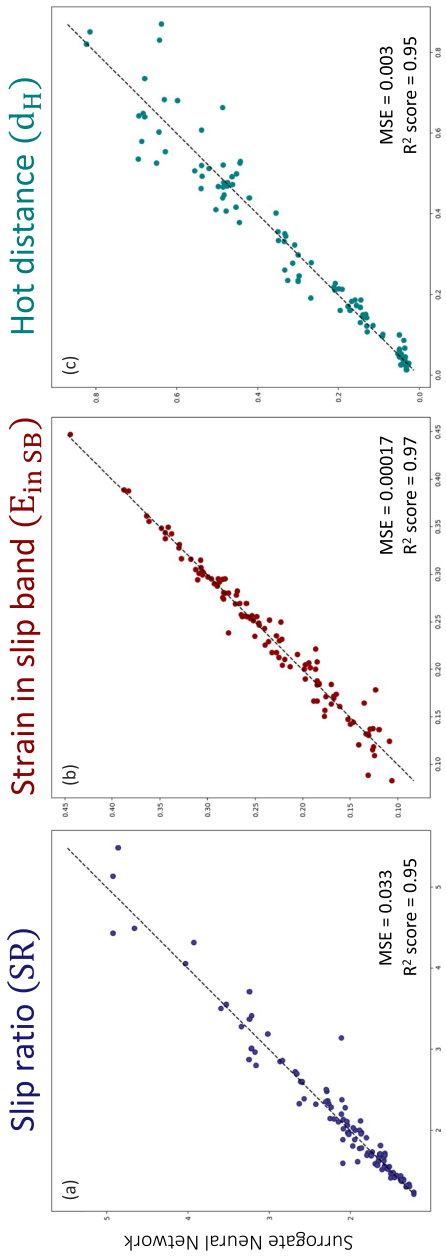

Fig. 9 Ground truth calculated by micromechanical simulation versus NN predicted values of three localization-based material properties, **a** average ratio of the strain accommodated by slip bands to that accommodated by grain matrices, **b** fraction of the total strain that is accommodated by slip bands, and **c** average normalized, adjusted distance between slip bands within the microstructure

create a fine grid of available values for our features, providing an applicable dataset for conducting a simple grid search for optimal material properties. An optimization algorithm may provide a more comprehensive search, but the grid search optimization used here is an easy and effective method that nearly continuously covers the space of input features considered.

For each localization-based property, box and whisker plots in Fig. 10 present the distribution of the 360 datapoints from our initial dataset. The optimal values obtained from the grid search are also indicated by yellow stars. To obtain each of these three values, we perform a micromechanical simulation on a 3D polycrystal we created using the optimal combination of microstructural features suggested by the grid search. This additional step verifies whether our data-driven optimization scheme produces a truthfully optimal localization response in Ti-6Al-4V. As shown in Fig. 10a, the optimal solution manifests a superior response, i.e., lower degree of localization. However, given that our initial dataset already contains samples with very low slip ratios and that the SR is lower-bound to 1.0, the gain from the optimal microstructure is not drastic. For the fraction of total strain accommodated by slip bands shown in Fig. 10b, the gain from the optimal microstructure is more pronounced, but still not significant. It should be noted, however, that a perfectly homogeneous distribution of deformation does not yield $E_{inSB} = 0$, as the slip band domains naturally occupy a few percent of the total microstructure. The most significant improvement in localization response is offered by the optimal solution that maximizes the hot distance. Figure 10c demonstrates the remarkable increase in the adjusted distance between intense slip bands in the polycrystal, achieved by the optimization scheme developed here.

Interestingly, we obtain a uniquely different optimal microstructure when considering each material property. That is to say, the microstructure configuration that maximizes the hot distance does not necessarily minimize the strain in slip bands. The polycrystal that minimizes the slip ratio (SR) has medium-sized, highly elongated grains with very small deviation in their size, and their orientation sampled from texture A. On the other

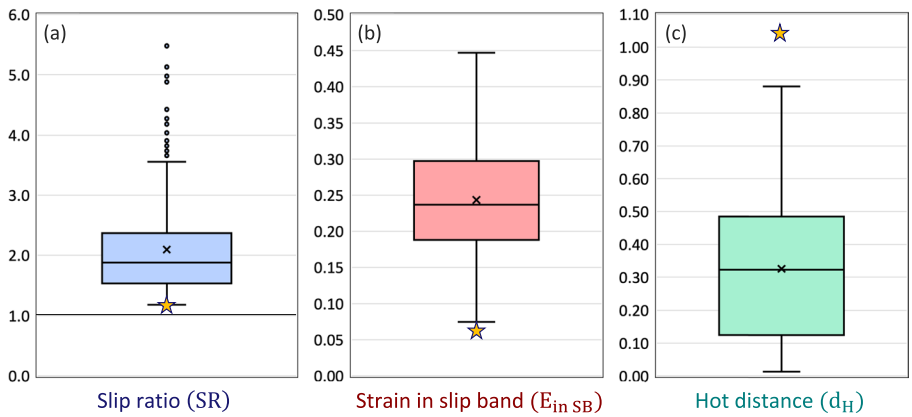

Fig. 10 Distribution of three localization-based material properties for 360 datapoints from our initial dataset, as well as three datapoints (indicated by yellow stars) obtained from micromechanical simulations on optimal solutions predicted by the data-driven optimization scheme. The set of microstructural features including texture, grain aspect ratio (AR), average grain size (ESD_{ave}), and standard deviation (σ) that optimize SR, E_{inSB}, and d_H are [A, 30, 21, 0.001], [F, 28, 52.5, 0.86], and [C, 30, 5, 0.02], respectively

hand, a polycrystal with texture F that comprises large grains that are highly dispersed in their size and elongated in their shape would minimize the fraction of the total strain localized within slip bands (E_{inSB}). Finally, the microstructure that maximizes the hot distance (d_H) is sampled from texture C, has small, yet again highly elongated, grains with small deviation in their size. In the next section, we further discuss these results.

Discussion

To represent the microstructure and create labels in our framework, we used the combination of a graph network and a simple neural network model. The graph network was used to account for grain neighborhood and connectivity throughout the polycrystal. Using this approach, we presented each microstructure with a total of four key features. Therefore, the input dimensionality was significantly reduced compared to voxel-based machine learning models such as convolutional neural networks (CNN) (Herriott and Spear 2020; Rao and Liu 2020; Li et al. 2019; Cecen et al. 2018; Yang et al. 2018) and graph neural network (GNN) models (Dai et al. 2021; Shu et al. 2022; Pagan et al. 2022; Hestroffer et al. 2023; Vlassis et al. 2020), leading to improved efficiency in terms of computation and memory requirements. While extracting the value of hot distance (d_H) in our approach is accomplished by applying a graph network to the polycrystal, the time required for training our NN models is significantly reduced compared to CNN and GNN models, for which the training time exponentially increases with the number of voxels and grains in the microstructure. Furthermore, the meticulously architectured, fully connected NN model used in this work successfully captures the intertwined effects of microstructural features on slip localization, an advantage that simpler methods such as non-linear regression with polynomials and splines fail to provide.

Another advantage of the model developed here is the interpretability of the features and labels, rendering our results readily applicable, from a manufacturing perspective. Although voxel-based CNNs retain the microstructural features for each voxel within the polycrystal, they fail to account for grain neighborhood, a critical aspect for determining macroscopic properties of polycrystalline materials (Herriott and Spear 2020; Khorrami et al. 2023; Cang et al. 2018). Furthermore, since the solution would include features, such as orientation, optimized for each voxel, an optimal microstructure one would get from a CNN is not deemed readily manufacturable. Recently, application of GNNs for predicting mechanical properties of polycrystalline materials have shown promising results in circumventing the first issue (Dai et al. 2021; Shu et al. 2022; Pagan et al. 2022; Hestroffer et al. 2023). Nevertheless, we anticipate that the interpretability of optimal solutions would remain challenging. With the current manufacturing capacities, creating a set of grains with orientations, morphology, and connectivity exactly as prescribed by the GNN is unfeasible. The optimal solution provided by our approach, on the other hand, is easy to interpret and feasible to manufacture as many experimental works have successfully developed techniques to control grain size, morphology, and texture in titanium alloys (Stubbington and Bowen 1974; Ng et al. 2022; Ao et al. 2020; Zhu et al. 1997; Murty and Charit 2006).

A disadvantage of feedforward NN models compared to GNNs is their underperformance when extrapolating in nonlinear tasks. However, studies show that the extrapolation capacity of MLPs enhances when the training distribution is diverse (Xu et al.

2020). We have verified this by conducting micromechanical simulations on polycrystals that were sampled from optimal solutions predicted by our NN models. While the improvement in some cases is only marginally significant, the solution microstructures produce localization responses that exceed the limits established from simulation of the initial dataset. This indicates that the trained NN models performed reasonably well when applied to the generated dataset.

We showed that the optimal microstructure designed for each localization-based property is unique with a set of microstructural features that does not optimize other properties. Surprisingly, one solution recommended texture F (uniformly random or no texture) with large grains to minimize the total strain localized within slip bands, while the solution that maximized the hot distance featured a rolling texture with small grains. Since the latter includes both the intensity of slip bands and the distance between intense slip bands within the microstructure, we may consider the optimal solution for hot distance more preferable. Ti-6Al-4V microstructures with smaller grains have also been experimentally associated with superior fatigue properties (Stubbington and Bowen 1974; Peters and Lütjering 1983; Kimura et al. 1980), arguably due to the fact that slip length and intensity is smaller in fine-grained materials.

Remarkably, a feature that was common in all optimal microstructures is the elongated shape of grains. This result suggests that higher grain aspect ratios lead to an improvement in localization-based properties, or equivalently, a more delocalized strain distribution in the material. A plausible argument here is that the smaller dimension in elongated grains can drastically reduce the likelihood of slip band formation and localization, if the orientation of the grain favors a slip band that spans along that direction. Therefore, not only will no slip band form in that grain which contributes to strain delocalization, but the grain will undergo either homogeneous or no deformation at all, breaking the potential chain of long-range localization in the microstructure.

As a final remark, given the close relationship between microscopic localization response and macroscopic material properties, and thanks to the current advances in novel manufacturing techniques, it is envisioned that the findings of this work provide valuable target features for designing optimal Ti-6Al-4V polycrystals to overcome the strength-toughness trade-off. Incorporating more possible textures and microstructural features, allowing slip bands to develop on multiple slip systems, and inclusion of the β phase in the microstructure can provide further insights in future works.

Conclusions

The development, long-range transmission, and connectivity of slip bands in polycrystalline materials including Ti-6Al-4V titanium alloy are experimentally evidenced to contribute to crack initiation and propagation (Echlin et al. 2016; Le Biavant et al. 2002). In this paper, we combined explicit slip band micromechanical simulations on 3D polycrystals with graph networks and neural network models to design a Ti-6Al-4V microstructure that features strain delocalization to some extent. This unique approach enabled us to circumvent the time-intensive search for optimal microstructures through mechanical simulations. Additionally, it accounted for the grain neighborhood and connectivity within the polycrystal and provided a level of interpretability that were otherwise missed if neural networks and graph neural networks were used alone. We first generated a

dataset of 3D polycrystals with different microstructural characteristics and ran crystal plasticity simulations to calculate the mechanical response of each polycrystal, from a localization standpoint. Motivated by the simulation results, we then formulated a set of localization-based properties to optimize, all in line with strain delocalization. These properties included the ratio of slip accumulated in slip bands to that in parent matrices, the fraction of total applied strain accommodated by slip bands, and the spatial connectivity of slip bands throughout the polycrystal. Separate neural network (NN) models were designed and tuned to predict these properties for a given set of microstructural features, such as texture, grain size and shape. Once the models are shown to be highly accurate, we employed them to generate additional data to enrich our initial, relatively limited dataset of 3D microstructures. Finally, we performed a grid search optimization on the new dataset to find optimal microstructures, each improving one property. The surrogate neural network models exhibited a promising predictive performance for localization-based properties. The optimization results identified that each material property is optimized by a unique microstructure solution. Remarkably, elongated grain shape emerged as a recurring feature among all optimal microstructures. These findings can help design polycrystalline Ti alloys that exhibit more homogeneous deformation and possess superior mechanical properties, such as strength and toughness.

Acknowledgements
B. A. and I. J. B. are grateful for support by the National Science Foundation under Grant Number 2051390. J. M. H. is grateful for the support by the U.S. Dept. of Energy, Office of Basic Energy Sciences Program DE-SC0018901. Use was made of computational facilities purchased with funds from the National Science Foundation (CNS-1725797) and administered by the Center for Scientific Computing (CSC). The CSC is supported by the California NanoSystems Institute and the Materials Research Science and Engineering Center (MRSEC; NSF DMR 2308708) at UC Santa Barbara.

Authors' contributions
B.A.: Conceptualization, Methodology, Formal analysis, Investigation, Visualization, Writing - original draft. A.L.B.: Writing - review & editing, Discussion. J.M.H.: Writing - review & editing, Discussion. M.AK: Writing- review & editing, Discussion. I.J.B: Conceptualization, Investigation, Writing - review & editing, Supervision, Funding acquisition. All authors reviewed the final version of the manuscript.

Funding
This work was supported by the National Science Foundation under Grant Number 2051390 and the U.S. Dept. of Energy, Office of Basic Energy Sciences under Grant Number DE-SC0018901. Use was made of computational facilities purchased with funds from the National Science Foundation (CNS-1725797) and administered by the Center for Scientific Computing (CSC). The CSC is supported by the California NanoSystems Institute and the Materials Research Science and Engineering Center (MRSEC; NSF DMR 2308708) at UC Santa Barbara.

Availability of data and materials
The datasets generated and/or analysed during the current study are available in the GitHub repository, https://github.com/BehnamAhmadikia/PolyGraphNN.

Declarations

Competing interests
The authors declare no competing interests.

Received: 29 August 2023 Accepted: 2 February 2024
Published: 1 March 2024

References

B. Ahmadikia, M.A. Kumar, I.J. Beyerlein, Effect of neighboring grain orientation on strain localization in slip bands in hcp materials. Int. J. Plast. **144**, 103026 (2021)
B. Ahmadikia, O. Paraskevas, W. Van Hyning, J. Hestroffer, I.J. Beyerlein, C. Thrampoulidis, Data-driven texture design for reducing elastic and plastic anisotropy in titanium alloys. Acta Mater. **265**, 119585 (2024). https://doi.org/10.1016/j.actamat.2023.119585
B. Ahmadikia, L. Wang, M.A. Kumar, I.J. Beyerlein, Grain boundary slip–twin transmission in titanium. Acta Mater. **244**, 118556 (2023)

D. Ao, J. Gao, X. Chu, S. Lin, J. Lin, Formability and deformation mechanism of Ti-6Al-4V sheet under electropulsing assisted incremental forming. Int. J. Solids Struct. **202**, 357–367 (2020)
R. Boyer, Attributes, characteristics, and applications of titanium and its alloys. JOM **62**, 21–24 (2010)
F. Bridier, D.L. McDowell, P. Villechaise, J. Mendez, Crystal plasticity modeling of slip activity in Ti-6Al-4V under high cycle fatigue loading. Int. J. Plast. **25**(6), 1066–1082 (2009)
F. Bridier, P. Villechaise, J. Mendez, Slip and fatigue crack formation processes in an α/β titanium alloy in relation to crystallographic texture on different scales. Acta Mater. **56**(15), 3951–3962 (2008)
R. Cang, H. Li, H. Yao, Y. Jiao, Y. Ren, Improving direct physical properties prediction of heterogeneous materials from imaging data via convolutional neural network and a morphology-aware generative model. Comput. Mater. Sci. **150**, 212–221 (2018)
A. Cecen, H. Dai, Y.C. Yabansu, S.R. Kalidindi, L. Song, Material structure-property linkages using three-dimensional convolutional neural networks. Acta Mater. **146**, 76–84 (2018)
S. Clark, P. Hayes. SigOpt Web page. (2019). https://sigopt.com. Accessed 25 July 2023
M. Dai, M.F. Demirel, Y. Liang, J.M. Hu, Graph neural networks for an accurate and interpretable prediction of the properties of polycrystalline materials. npj Comput. Mater. **7**(1), 103 (2021)
P.R. Dawson, M.P. Miller, T.M. Pollock, J. Wendorf, L.H. Mills, J.C. Stinville, M.A. Charpagne, M.P. Echlin, Mechanical metrics of virtual polycrystals (mechmet). Integrating Mater. Manuf. Innov. **10**, 265–285 (2021)
M.P. Echlin, J.C. Stinville, V.M. Miller, W.C. Lenthe, T.M. Pollock, Incipient slip and long range plastic strain localization in microtextured Ti-6Al-4V titanium. Acta Mater. **114**, 164–175 (2016)
C. Erel, G. Po, N. Ghoniem, Dependence of hardening and saturation stress in persistent slip bands on strain amplitude during cyclic fatigue loading. Phil. Mag. **97**(32), 2947–2970 (2017)
N.M. Ghoniem, E.P. Busso, N. Kioussis, H. Huang, Multiscale modelling of nanomechanics and micromechanics: an overview. Phil. Mag. **83**(31–34), 3475–3528 (2003)
M.A. Groeber, M.A. Jackson, DREAM. 3D: a digital representation environment for the analysis of microstructure in 3D. Integrating Mater. Manuf. Innov. **3**, 56–70 (2014)
A. Hagberg, P. Swart, D. S Chult, Exploring network structure, dynamics, and function using networkx. Tech. rep., Los Alamos National Lab.(LANL), Los Alamos, NM (United States) (2008)
S. Hémery, A. Nait-Ali, M. Guéguen, J. Wendorf, A. Polonsky, M. Echlin, J. Stinville, T. Pollock, P. Villechaise, A 3D analysis of the onset of slip activity in relation to the degree of micro-texture in Ti-6Al-4V. Acta Mater. **181**, 36–48 (2019)
S. Hémery, P. Nizou, P. Villechaise, In situ sem investigation of slip transfer in Ti-6Al-4V: Effect of applied stress. Mater. Sci. Eng. A **709**, 277–284 (2018)
C. Herriott, A.D. Spear, Predicting microstructure-dependent mechanical properties in additively manufactured metals with machine-and deep-learning methods. Comput. Mater. Sci. **175**, 109599 (2020)
J.M. Hestroffer, M.A. Charpagne, M.I. Latypov, I.J. Beyerlein, Graph neural networks for efficient learning of mechanical properties of polycrystals. Comput. Mater. Sci. **217**, 111894 (2023)
X. Hu, Y. Ji, L. Chen, R.A. Lebensohn, L.Q. Chen, X. Cui, Spectral phase-field model of deformation twinning and plastic deformation. Int. J. Plast. **143**, 103019 (2021)
M.S. Khorrami, J.R. Mianroodi, N.H. Siboni, P. Goyal, B. Svendsen, P. Benner, D. Raabe, An artificial neural network for surrogate modeling of stress fields in viscoplastic polycrystalline materials. npj Comput. Mater. **9**(1), 37 (2023)
H. Kimura, O. Izumi, *Titanium'80, Science and Technology*, vol. 1 (Metallurgical Society of AIME, Kyoto, 1980), p.1980
D.P. Kingma, J. Ba, Adam: A method for stochastic optimization. (2014). arXiv preprint arXiv:1412.6980.
M.A. Kumar, I.J. Beyerlein, Influence of plastic properties on the grain size effect on twinning in Ti and Mg. Mater. Sci. Eng. A **771**, 138644 (2020)
M.A. Kumar, I.J. Beyerlein, C.N. Tomé, Effect of local stress fields on twin characteristics in HCP metals. Acta Mater. **116**, 143–154 (2016a)
M.A. Kumar, I.J. Beyerlein, C.N. Tomé, Grain size constraints on twin expansion in hexagonal close packed crystals. J. Appl. Phys. **120**(15), 155105 (2016b)
M.A. Kumar, L. Capolungo, R. McCabe, C. Tomé, Characterizing the role of adjoining twins at grain boundaries in hexagonal close packed materials. Sci. Rep. **9**(1), 3846 (2019)
C. Lavogiez, S. Hémery, P. Villechaise, Concurrent operation of $< c + a >$ slip and twinning under cyclic loading of Ti-6Al-4V. Scr. Mater. **157**, 30–33 (2018)
K. Le Biavant, S. Pommier, C. Prioul, Local texture and fatigue crack initiation in a Ti-6Al-4V titanium alloy. Fatigue Fract. Eng. Mater. Struct. **25**(6), 527–545 (2002)
R.A. Lebensohn, A.K. Kanjarla, P. Eisenlohr, An elasto-viscoplastic formulation based on fast fourier transforms for the prediction of micromechanical fields in polycrystalline materials. Int. J. Plast. **32**, 59–69 (2012)
X. Li, Z. Liu, S. Cui, C. Luo, C. Li, Z. Zhuang, Predicting the effective mechanical property of heterogeneous materials by image based modeling and deep learning. Comput. Methods Appl. Mech. Eng. **347**, 735–753 (2019)
R. Liu, A. Kumar, Z. Chen, A. Agrawal, V. Sundararaghavan, A. Choudhary, A predictive machine learning approach for microstructure optimization and materials design. Sci. Rep. **5**(1), 1–12 (2015)
D. Lunt, J.Q.D. Fonseca, D. Rugg, M. Preuss, in *Proceedings of the 13th World Conference on Titanium*. Slip band characterisation in Ti-6Al-4V with varying degrees of macrozones (Hoboken, John Wiley & Sons, Inc., 2016), pp. 1129–1134
G. Lütjering, Influence of processing on microstructure and mechanical properties of ($\alpha+\beta$) titanium alloys. Mater. Sci. Eng. A **243**(1–2), 32–45 (1998)
A. Mangal, E.A. Holm, Applied machine learning to predict stress hotspots ii: Hexagonal close packed materials. Int. J. Plast. **114**, 1–14 (2019)
A. Marano, L. Gélébart, S. Forest, Intragranular localization induced by softening crystal plasticity: Analysis of slip and kink bands localization modes from high resolution FFT-simulations results. Acta Mater. **175**, 262–275 (2019)
A. Marano, L. Gélébart, Non-linear composite voxels for FFT-based explicit modeling of slip bands: application to basal channeling in irradiated Zr alloys. Int. J. Solids Struct. **198**, 110–125 (2020)
K.L. Murty, I. Charit, Texture development and anisotropic deformation of zircaloys. Prog. Nucl. Energy **48**(4), 325–359 (2006)

C. Ng, M. Bermingham, M. Dargusch, Controlling grain size, morphology and texture in additively manufactured β-titanium alloy with super transus hot isostatic pressing. Additive Manuf. **59**, 103176 (2022)
D.C. Pagan, C.R. Pash, A.R. Benson, M.P. Kasemer, Graph neural network modeling of grain-scale anisotropic elastic behavior using simulated and measured microscale data. npj Comput. Mater. **8**(1), 259 (2022)
S. Papanikolaou, Y. Cui, N. Ghoniem, Avalanches and plastic flow in crystal plasticity: an overview. Model. Simul. Mater. Sci. Eng. **26**(1), 013001 (2017)
M. Peters, A. Gysler, G. Lütjering, Influence of texture on fatigue properties of Ti-6Al-4V. Metall. Mater. Trans. A **15**, 1597–1605 (1984)
M. Peters, G. Lütjering, P183 of titanium and titanium alloys, report cs-2933. Electr. Power Res. Inst. (1983)
M. Peters, G. Lütjering, G. Ziegler, Control of microstructures of $(\alpha+\beta)$-titanium alloys. Int. J. Mater. Res. **74**(5), 274–282 (1983)
M.W. Priddy, S.R. Kalidindi, D. McDowell, N. Paulson, Synthetic alpha-Ti microstructures and associated elastic stiffness and yield strength properties-extended. matin.gatech.edu/resources/187 (2017)
C. Rao, Y. Liu, Three-dimensional convolutional neural network (3D-CNN) for heterogeneous material homogenization. Comput. Mater. Sci. **184**, 109850 (2020)
Y.M. Ren, X. Lin, X. Fu, H. Tan, J. Chen, W. Huang, Microstructure and deformation behavior of Ti-6Al-4V alloy by high-power laser solid forming. Acta Mater. **132**, 82–95 (2017)
C. Shu, J. He, G. Xue, C. Xie, Grain knowledge graph representation learning: A new paradigm for microstructure-property prediction. Crystals **12**(2), 280 (2022)
G. Simmons, H. Wang. Single crystal elastic constants and caluculated aggregate properties. A handbook, vol. 4 (MIT press, 1971)
B.D. Smith, Microstructure-sensitive plasticity and fatigue of three titanium alloy microstructures. Ph.D. thesis, Georgia Institute of Technology (2013)
J. Stinville, M. Charpagne, A. Cervellon, S. Hemery, F. Wang, P. Callahan, V. Valle, T. Pollock, On the origins of fatigue strength in crystalline metallic materials. Science **377**(6610), 1065–1071 (2022)
C. Stubbington, A. Bowen, Improvements in the fatigue strength of Ti-6Al-4V through microstructure control. J. Mater. Sci. **9**, 941–947 (1974)
N.N. Vlassis, R. Ma, W. Sun, Geometric deep learning for computational mechanics part i: Anisotropic hyperelasticity. Comput. Methods Appl. Mech. Eng. **371**, 113299 (2020)
H. Wang, B. Clausen, L. Capolungo, I.J. Beyerlein, J. Wang, C.N. Tome, Stress and strain relaxation in magnesium AZ31 rolled plate: In-situ neutron measurement and elastic viscoplastic polycrystal modeling. Int. J. Plast. **79**, 275–292 (2016)
Q. Wang, Z. Liu, Plastic deformation induced nano-scale twins in Ti-6Al-4V machined surface with high speed machining. Mater. Sci. Eng. A **675**, 271–279 (2016)
J. Wang, M. Zecevic, M. Knezevic, I.J. Beyerlein, Polycrystal plasticity modeling for load reversals in commercially pure titanium. Int. J. Plast. **125**, 294–313 (2020)
J.C. Williams, R.R. Boyer, Opportunities and issues in the application of titanium alloys for aerospace components. Metals **10**(6), 705 (2020)
K. Xu, M. Zhang, J. Li, S.S. Du, K.i. Kawarabayashi, S. Jegelka, How neural networks extrapolate: From feedforward to graph neural networks. arXiv preprint arXiv:2009.11848. (2020)
Z. Yang, Y.C. Yabansu, R. Al-Bahrani, W.K. Liao, A.N. Choudhary, S.R. Kalidindi, A. Agrawal, Deep learning approaches for mining structure-property linkages in high contrast composites from simulation datasets. Comput. Mater. Sci. **151**, 278–287 (2018)
G.G. Yapici, I. Karaman, Z.P. Luo, Mechanical twinning and texture evolution in severely deformed Ti-6Al-4V at high temperatures. Acta Mater. **54**(14), 3755–3771 (2006)
M. Yoo, Slip, twinning, and fracture in hexagonal close-packed metals. Metall. Trans. A **12**, 409–418 (1981)
M. Zhang, F. Bridier, P. Villechaise, J. Mendez, D. McDowell, Simulation of slip band evolution in duplex Ti-6Al-4V. Acta Mater. **58**(3), 1087–1096 (2010)
Z. Zhu, R. Liu, M. Yan, C. Cao, J. Gu, N. Chen, Texture control and the anisotropy of mechanical properties in titanium sheet. J. Mater. Sci. **32**(19), 5163–5167 (1997)

Publisher's Note